Teleoperation of Steerable Flexible Needles by Combining Kinesthetic and Vibratory Feedback

Claudio Pacchierotti, *Student Member, IEEE*,
Momen Abayazid, *Student Member, IEEE*,
Sarthak Misra, *Member, IEEE*, and
Domenico Prattichizzo, *Senior Member, IEEE*

Abstract—Needle insertion in soft-tissue is a minimally invasive surgical procedure that demands high accuracy. In this respect, robotic systems with autonomous control algorithms have been exploited as the main tool to achieve high accuracy and reliability. However, for reasons of safety and responsibility, autonomous robotic control is often not desirable. Therefore, it is necessary to focus also on techniques enabling clinicians to directly control the motion of the surgical tools. In this work, we address that challenge and present a novel teleoperated robotic system able to steer flexible needles. The proposed system tracks the position of the needle using an ultrasound imaging system and computes needle's ideal position and orientation to reach a given target. The master haptic interface then provides the clinician with mixed kinesthetic-vibratory navigation cues to guide the needle toward the computed ideal position and orientation. Twenty participants carried out an experiment of teleoperated needle insertion into a soft-tissue phantom, considering four different experimental conditions. Participants were provided with either mixed kinesthetic-vibratory feedback or mixed kinesthetic-visual feedback. Moreover, we considered two different ways of computing ideal position and orientation of the needle: with or without set-points. Vibratory feedback was found more effective than visual feedback in conveying navigation cues, with a mean targeting error of 0.72 mm when using set-points, and of 1.10 mm without set-points.

Index Terms—Computers and information processing, haptic interfaces, force feedback, engineering in medicine and biology, surgical instruments, biomedical equipment, hypodermic needles, biomedical imaging

1 Introduction

Needle insertion in soft-tissue is a minimally invasive surgical (MIS) procedure used for diagnostic and therapeutic purposes, and it is one of the many surgical procedures that may greatly benefit from the use of teleoperated robotic systems [1]. Inaccurate placement of the needle tip may, in fact, result in misdiagnosis or unsuccessful treatment during, for instance, biopsies or brachytherapies [1], [2]. Hence, researchers have been constantly trying to develop new techniques and systems able to enhance the accuracy of this type of needle insertions. Flexible needles are one of these technological advancements, introduced to provide enhanced steering capabilities. Several control algorithms have been developed for maneuvering flexible needles in two- and three-dimensional spaces. Duindam et al. developed a model to describe three-dimensional (3D) deflection of bevel-tipped flexible needles for path planning purposes [3], and Hauser et al. developed a 3D feedback controller to steer needles along a helical path [4]. However, results from both Duindam et al. and Hauser et al. were based solely on simulations, and no experiments in real scenarios were performed. More recently, Abayazid et al. presented a 2D ultrasound image-guided steering algorithm [5] and a 3D needle steering controller for bevel-tipped flexible needles [6], where they used Fiber Bragg Grating sensors to reconstruct the needle shape in real-time.

However, for reasons of safety and responsibility, it would be beneficial to provide clinicians with direct control of the motion of the medical instrument [7], [8]. In such a case, the clinician needs to observe, from the master side, the environment the needle is interacting with. This is possible through different types of information that flow from the remote scenario to the human operator. They are usually a combination of visual, auditory and haptic stimuli. Visual and auditory feedback are already employed in commercial robotic surgery systems (e.g., the da Vinci Si Surgical System) while it is not common to find commercially-available devices implementing haptic force feedback.

However, force feedback is widely considered to be a valuable navigation tool during teleoperated surgical procedures [9], [10]. It enhances clinicians' performance in terms of completion time of a given task [11], [12] , accuracy [9], [13], [14] , peak and mean applied force [11], [14], [15]. Force feedback also improves performance in fine microneedle positioning [10], telerobotic catheter insertion [16], and cardiothoracic procedures [17]. Moreover, haptic feedback can be also employed to *augment* the operating environment, providing additional valuable information to the clinician, such as navigation cues. For example, Nakao et al. [18] presented a haptic navigation method that allows clinicians to avoid collision with forbidden regions during surgery. It employs kinesthetic feedback through a 2D master manipulator. In addition to these approaches, which mostly involve kinesthetic force feedback, there is also a growing interest in vibratory feedback. Erp. et al. [19], for instance, employed a vibrating waist belt to provide navigation information to the user. More recently, Kuchenbecker et al. presented the Verro-Touch system [20], which measures the vibrations at the tip of the surgical tool and recreates them on the master handle.

1.1 Contributions

In this study we present an innovative teleoperation system for steering flexible needles. It enables clinicians to directly maneuver the surgical tool while providing them with navigation cues through kinesthetic and vibratory force feedback.

The ultrasound-guided tracking algorithm of Vrooijink et al. [21] tracks in real-time the needle tip and estimates its reachable region. The steering algorithm of Abayazid et al. [6] then computes ideal position and orientation of the needle to always keep the target in its reachable region. The master system uses this information to provide the clinician with haptic feedback about needle's ideal position and orientation. This information is provided as a combination of kinesthetic and vibratory force. A picture of the teleoperation system is reported in Fig. 1. Moreover, Fig. 2 shows how the master and slave systems are inter-connected. In addition to the description of the system, we present its evaluation in a paradigmatic needle steering task. We compared the performance of the proposed feedback approach (kinesthetic and vibratory) with a more popular feedback technique that combines kinesthetic and visual feedbacks. Our hypothesis is that providing both cues through the same sensory channel (haptic) performs better than providing the two cues through different sensory channels (haptic and visual).

1.1.1 Shared- vs. Autonomous-Control Systems

The main difference between the approach presented by Abayazid et al. and the one presented here is the role of the human operator. In the work of Abayazid et al., the controller has full control on the motion of the slave robot, applying the computed ideal position and orientation directly to the needle. No human is involved in the control loop. In our work, on the other hand, the controller still evaluates the ideal position and orientation of

- *C. Pacchierotti and D. Prattichizzo are with the Department of Information Engineering and Mathematics, University of Siena, and the Department of Advanced Robotics, Istituto Italiano di Tecnologia, Italy. E-mail: {pacchierotti, prattichizzo}@dii.unisi.it.*
- *M. Abayazid and S. Misra are with the Department of Biomechanical Engineering, MIRA—Institute for Biomedical Technology and Technical Medicine, University of Twente, The Netherlands. E-mail: {m.abayazid, s.misra}@utwente.nl.*

Manuscript received 9 June 2014; revised 10 Sept. 2014; accepted 21 Sept. 2014. Date of publication 23 Sept. 2014; date of current version 15 Dec. 2014.
Recommended for acceptance by R. Adams.
For information on obtaining reprints of this article, please send e-mail to: reprints@ieee.org, and reference the Digital Object Identifier below.
Digital Object Identifier no. 10.1109/TOH.2014.2360185

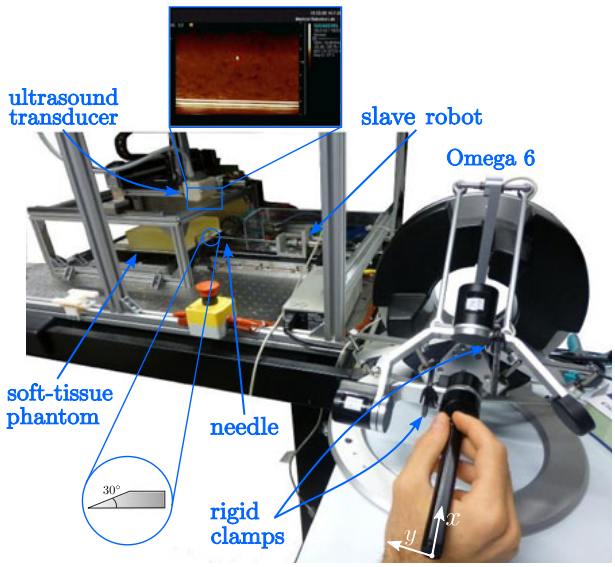

Fig. 1. Teleoperation system. Through the Omega 6 haptic device the clinician controls the motion of the slave robot and, thus, the needle. The haptic interface also provides the clinician with navigation cues about the ideal position and orientation of the needle tip, as evaluated by the steering algorithm.

the needle but does not directly control the needle's motion. Ideal position and orientation are provided to the master interface, which present them to the clinician, who, in turn, commands the slave robot and steers the needle toward its target point. The clinician has thus *full* control on the motion of the needle, and haptic feedback provides the necessary guiding information. The complexity of the flexible needle kinematics and medical scenario make haptic feedback a valuable support tool for guidance. Finally, to the best of our knowledge, no commercially-available surgical system provide such a rich pattern of information through the haptic channel.

2 Teleoperation System

The slave system consists of a bevel-tipped nitinol needle mounted on a two degrees-of-freedom (DOF) robotic device. The robot allows the needle to move along the direction of insertion and

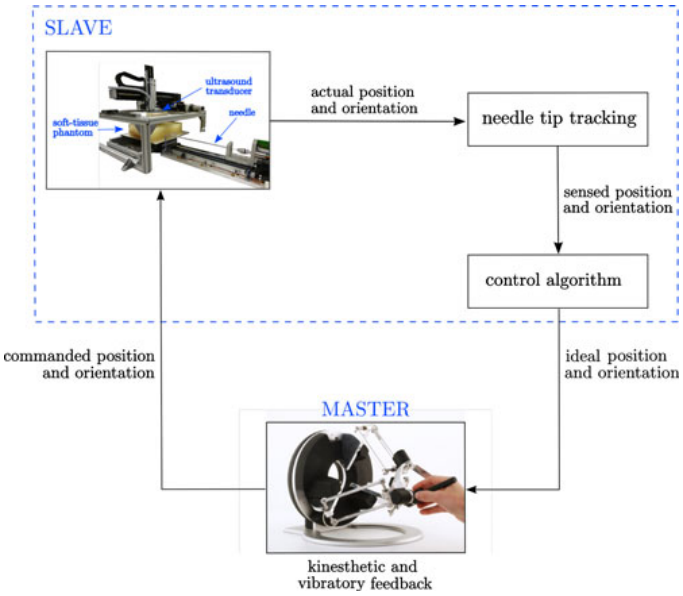

Fig. 2. Teleoperation system overview. The ultrasound-guided steering algorithm, presented in Section 3.1, computes the ideal position and orientation of the needle. The haptic interface provides this information to the clinician through a mix of kinesthetic and vibratory forces, as described in Section 3.2. The clinician then controls the motion of the slave robot from the master interface.

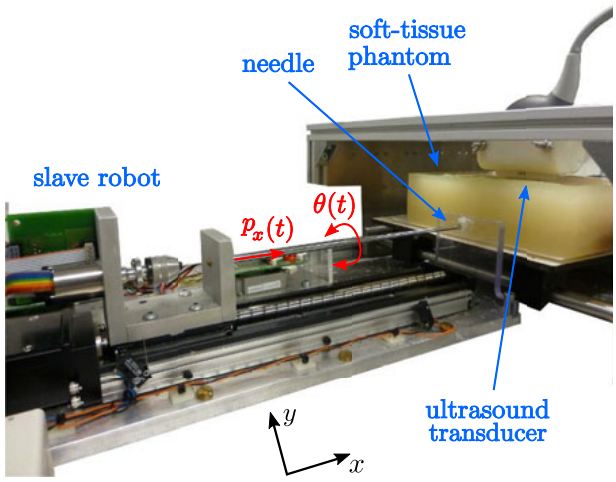

Fig. 3. Slave system. The two degrees-of-freedom robotic device steers the flexible needle according to the commanded position $p_x(t)$ and commanded orientation $\theta(t)$, provided by the master device. The ultrasound transducer allowed to track the needle during the insertion.

rotate about its axis (see Fig. 3). Moreover, an ultrasound-guided tracking system is used to determine needle tip position during the insertion. Needle's tracking is guaranteed by a 18 MHz ultrasound transducer mounted on a three DOF Cartesian robot, which follows the needle tip during the insertion. The transducer is connected to a Siemens Acuson S2000 ultrasound machine. The steering and tracking algorithms are summarized in Section 3.1.

The master system consists of the single-contact grounded haptic interface Omega 6 (Force Dimension, Switzerland), shown in Fig. 4. Two rigid clamps prevent the wrist of the haptic device from moving. The actuators then block two additional DOF, resulting in a haptic interface with 2 DOF, one active (translation in the x direction) and one passive (rotation of the pen-shaped end-effector about the x-axis). The master interface allows the clinician to steer the needle and provides her with navigation cues through kinesthetic and vibratory force feedback. The haptic rendering algorithm is detailed in Section 3.2.

Communication between the slave and the master systems is set up through a User Datagram Protocol over IP (UDP/IP) socket connection on an Ethernet Local Area Network (LAN). The stability of the teleoperation system is guaranteed by the passivity-based approach presented by Franken et al. [22].

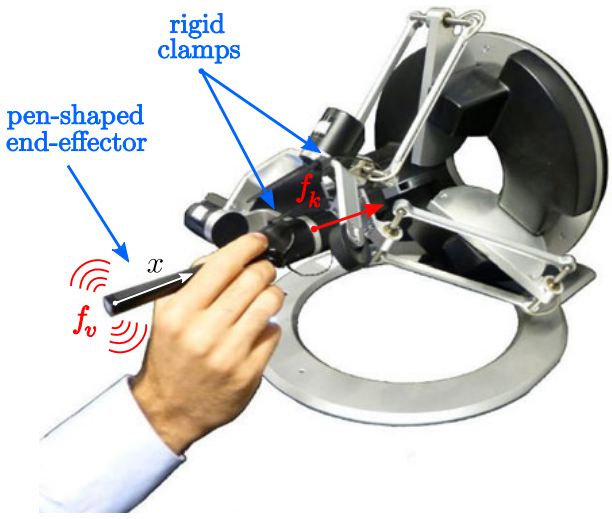

Fig. 4. Kinesthetic-vibratory feedback. The Omega 6 haptic interface enables the operator to directly steer the needle while being provided with kinesthetic force $\mathbf{f_k}$ and vibratory force $\mathbf{f_v}$ about needle's ideal position and orientation, respectively. The motion of the haptic device is constrained along its x-axis (white arrow). This feedback modality provides no visual information.

3 METHODS

3.1 Slave System

The slave system is in charge of tracking and steering the needle during its insertion into the soft-tissue phantom.

The needle tip tracking algorithm estimates the 3D needle tip pose intra-operatively through a 2D ultrasound transducer [21]. On the other hand, the steering control algorithm, starting from the estimated needle pose, computes the ideal position and orientation of the needle to reach the given target. More details about the steering algorithm can be found in the work by Abayazid et al. [6]. A modified version of this algorithm consists in steering the needle toward the final target through a sequence of preceding points, which we referred to as *set-points* [23]. As the needle tip reaches a set-point, the next one is automatically set to be the goal, and so on, until, eventually, the only point left is the final target. In both cases, the algorithm provides the haptic interface with the reference signals at 25 Hz, which is the refresh rate of the ultrasound machine.

3.2 Master System

The master system is in charge of steering the slave robot and displaying navigation cues to the clinician, i.e., ideal position and orientation of the needle as computed by the control algorithm. In order to avoid confusion, and consequent possible errors in the medical intervention, the meaning of such cues must be easy to understand.

In this paper we propose to provide the clinician with a combination of kinesthetic and vibratory feedback, as detailed in Section 3.2.1. Conveying information solely through the haptic channel leaves, in fact, other sensory channels free. For example, an operator teleoperating a needle using this feedback condition may also be provided with additional visual information (e.g., an ultrasound image of the needle). Moreover, we expect it to be more effective than providing multiple cues through different sensory channels. For this reason, we decided to compare our mixed kinesthetic-vibratory approach to a different combination of stimuli. This second feedback modality provides the operator with a combination of kinesthetic and visual feedback, as detailed in Section 3.2.2.

3.2.1 Mixing Kinesthetic and Vibratory Feedback

Combining multiple haptic stimuli to convey both ideal position and orientation of the needle is an interesting and promising choice. It leaves other sensory channels free and uses a single interface to both steer the slave robot and display navigation cues to the operator. However, it has to face the challenging problem of conveying two stimuli through the haptic sensory channel.

In order to differentiate those stimuli, we propose to provide the operator with

i) kinesthetic force $\mathbf{f_k}$ to convey information about the ideal *position* of the needle tip,
ii) vibratory force $\mathbf{f_v}$ to convey information about the ideal *orientation* of the needle tip,

as depicted in Fig. 4. Ideal position $p_{i,x}(t) \in \Re$ and ideal orientation $\theta_i(t) \in \Re$ at time t are computed by the steering algorithm as described in Section 3.1.

Kinesthetic force feedback along the x-axis is controlled by a penalty function based on the distance between the position of the haptic probe $\mathbf{p(t)} = \begin{bmatrix} p_x(t) & p_y(t) & p_z(t) \end{bmatrix}^{\mathrm{T}} \in \Re^{3\mathrm{x}1}$ and the current ideal position $p_{i,x}(t)$, while the motion along the y and z axes is blocked:

$$\mathbf{f_k} = \mathbf{K}\,\mathbf{D(t)} - \mathbf{B}\,\dot{\mathbf{D}}(\mathbf{t}), \tag{1}$$

where $\mathbf{B} = 1.5\,\mathbf{I_3}$ Ns/m, $\mathbf{K} = \mathrm{diag}[1 \;\; 4 \;\; 4]$ N/mm, and $\mathbf{D} = \mathbf{p_i(t)} - \mathbf{p(t)}$ is the distance between the ideal position $\mathbf{p_i(t)} = [p_{i,x}(t) \;\; 0.10 \;\; 0.08]^{\mathrm{T}}$ m and the current position of the haptic probe. The motion is thus limited along the x-axis and a kinesthetic force guides the operator toward $p_{i,x}(t)$. Reference position $\mathbf{p_i(t)}$ along the y and z axis was chosen to keep the end-effector of the Omega interface equidistant from its three actuators (as in Fig. 4).

On the other hand, information concerning the orientation of the needle tip is provided through vibratory feedback. It is controlled by a penalty function based on the difference between the ideal orientation $\theta_i(t)$ and the current orientation of the haptic probe $\theta(t) \in \Re$:

$$\mathbf{f_v} = \mathbf{A_1}|\theta_i(t) - \theta(t)| \quad \mathrm{sgn}(\sin(\omega t)), \tag{2}$$

where $\mathbf{A_1} = \frac{3}{\pi}\,\mathbf{I_{3x1}}$ N/rad and

$$\omega = \begin{cases} 200 \;\; \mathrm{Hz} & \text{if } \theta(t) - \theta_i(t) \geq 0, \\ 150 \;\; \mathrm{Hz} & \text{if } \theta(t) - \theta_i(t) < 0. \end{cases}$$

Vibrations thus provide information about the ideal orientation $\theta_i(t)$, indicating in which direction and how much the clinician should rotate the pen-shaped haptic probe. Frequency ω indicates in which direction the clinician should rotate the pen-shaped haptic probe: clockwise for $\omega = 200$ Hz and counter-clockwise for $\omega = 150$ Hz. Frequency values are chosen to maximally stimulate the Pacinian corpuscle receptors [24], be easy to distinguish [25] and fit the master device specifications. On the other hand, the amplitude of these vibrations indicates how much the clinician should rotate the haptic probe: no vibrations indicated the best performance. Amplitude scaling matrix $\mathbf{A_1}$ is chosen to maximize the just-noticeable difference [26] for the error $|\theta_i(t) - \theta(t)|$ and fit the master device specifications.

The total force provided to the operator through the Omega 6 haptic interface is then evaluated by combining eq. (1) and (2),

$$\mathbf{f_{t,1}} = \mathbf{f_k} + \mathbf{f_v}. \tag{3}$$

The operator is asked to keep the magnitude of $\mathbf{f_{t,1}}$ as small as possible, since a null value of this force denotes the least error. The haptic interface refresh rate is 1 kHz.

3.2.2 Mixing Kinesthetic Force and Visual Feedback

In order to better evaluate the effectiveness of our mixed kinesthetic-vibratory approach, we compared it to a different combination of stimuli, employing a popular visual feedback technique [9]. In this alternative feedback condition we provide the operator with

i) kinesthetic force $\mathbf{f_k}$ to convey information about the ideal *position* of the needle tip (as in the previous kinesthetic-vibratory approach),
ii) visual feedback to convey information about the ideal *orientation* of the needle tip,

as depicted in Fig. 5. Ideal position $p_{i,x}(t) \in \Re$ and ideal orientation $\theta_i(t) \in \Re$ at time t are again computed by the steering algorithm as described in Section 3.1.

Kinesthetic force feedback is computed as in the kinesthetic-vibratory modality (see eq. (1)). The motion is again limited along the x-axis and a kinesthetic force guides the operator toward $p_{i,x}(t)$. Moreover, since this time kinesthetic force is the only force applied to the operator, we can define the total force provided through the Omega 6 simply as

$$\mathbf{f_{t,2}} = \mathbf{f_k}. \tag{4}$$

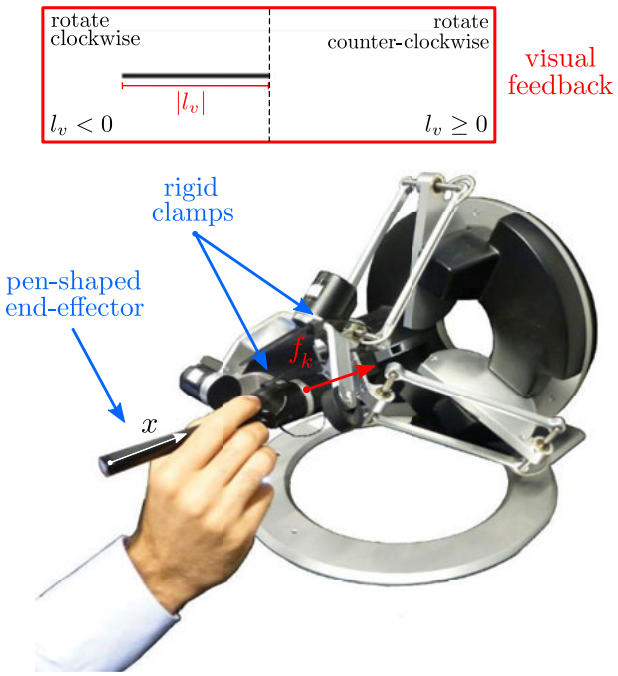

Fig. 5. Kinesthetic-visual feedback. The Omega 6 haptic interface enables the operator to directly steer the needle while being provided with kinesthetic force $\mathbf{f_k}$ and visual feedback about needle's ideal position and orientation, respectively.

On the other hand, information concerning the orientation of the needle tip is now provided through visual feedback. A black horizontal bar shows on the screen the difference between the ideal orientation $\theta_i(t)$ and the current orientation of the haptic probe $\theta(t)$. Its height is fixed to 5 mm and its width varies as

$$l_v = A_2(\theta_i(t) - \theta(t)),$$

where $A_2 = \frac{10}{\pi}$ cm/rad. The operator is asked to keep l_v as small as possible, since a null value of the bar width denotes the least error. If $l_v < 0$ the bar grows on the left, and the operator thus needs to rotate the pen-shaped end-effector clockwise (as in Fig. 5). Otherwise, if $l_v \geq 0$, the bar grows on the right, and the operator is required to rotate the end-effector counter-clockwise. Amplitude scaling matrix A_2 is chosen to provide good sensitivity to the error $|\theta_i(t) - \theta(t)|$ and be seen in one glance, without the need of rotating the head.

4 Experimental Evaluation

This section presents the experimental validation of the integrated teleoperation system. The experimental setup is shown in Figs. 1. It is composed of the slave and master systems described in Section 2. The slave robot steers a flexible nitinol alloy needle with a diameter of 0.5 mm and a bevel angle (at the tip) of 30°. The needle is inserted into a soft-tissue phantom made of gelatine mixture, to which silica powder is added to mimic the acoustic scattering of human tissue [6].

We tested our system while providing the subjects with either the kinesthetic-vibratory modality presented in Section 3.2.1 or the kinesthetic-visual modality presented in Section 3.2.2. Moreover, we considered two different ways of computing ideal position and orientation of the needle: with or without set-points (see Section 3.1).

4.1 Teleoperation of Flexible Needles

Twenty participants (12 males, eight females, age range 23-56 years) took part in the experiment, all of whom were right-handed. Four of them had previous experience with haptic interfaces. None of them had experience in the medical field. None reported any deficiencies in their perception abilities.

The task consisted of steering the needle toward a given target point, located at $\mathbf{o_t} = [85\ -10\ \ 5]^{\mathrm{T}}$ mm with respect to the initial position of the needle (see Fig. 3). The control algorithm calculates the ideal position and orientation of the needle tip using either set-points or not, as discussed in Section 3.1. The haptic interface presents these two pieces of information either via kinesthetic-vibratory feedback or kinesthetic-visual feedback, as discussed in Section 3.2. The operator then steers the needle, relying only on these navigation cues. A video of the experiment can be downloaded from http://goo.gl/KRE51k. Each participant made four randomized trials of the needle steering task, with one repetition for each condition proposed:

i) kinesthetic-vibratory feedback with ideal position and orientation calculated using set-points (VB+S),
ii) kinesthetic-vibratory feedback with ideal position and orientation calculated without using set-points (VB),
iii) kinesthetic-visual feedback with ideal position and orientation calculated using set-points (VI+S),
iv) kinesthetic-visual feedback with ideal position and orientation calculated without using set-points (VI).

In order to avoid providing undesired auditory cues, participants were isolated from external noises through a pair of noise-cancelling headphones. Participants were informed about the procedure before the beginning of the experiment and a 10-minute familiarization period was provided to make them acquainted with the experimental setup. The mean error in reaching the target point e_t, and the mean errors over time in following the ideal position and orientation signals, e_p and e_o, provided a measure of accuracy. Error e_t is calculated as $\|\mathbf{n_f} - \mathbf{o_t}\|$, where $\mathbf{n_f} \in \Re^{3x1}$ represents needle tip position at the end of the task. Errors on the ideal signals, e_p and e_o, are computed as the mean over time of $\|p_x(t) - p_{i,x}(t)\|$ and $\|\theta(t) - \theta_i(t)\|$, respectively. A null value of these three metrics denotes the best performance.

Fig. 6a shows targeting error e_t for the four experimental conditions. The collected data passed Shapiro-Wilk normality test but not Levene's homogeneity test. Comparison of the means among the feedback modalities was thus tested using Welch ANOVA. The

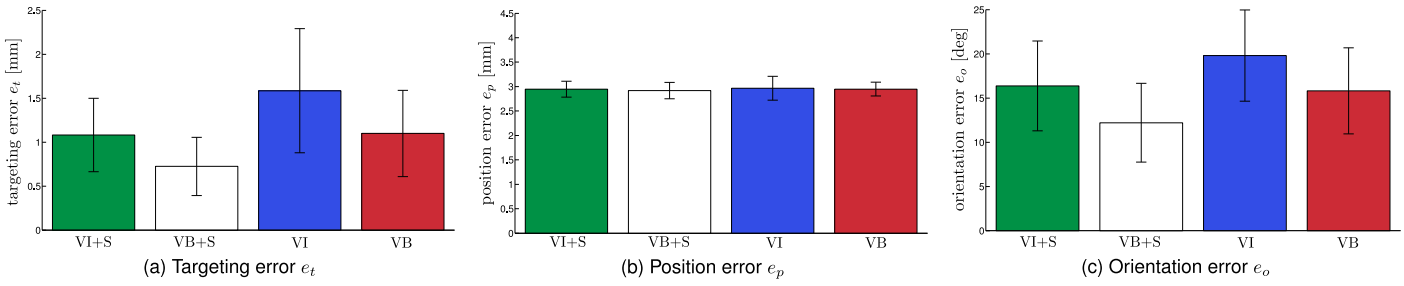

Fig. 6. Needle insertion experiment. (a) Targeting error e_t, (b) position error e_p, and (c) orientation error e_o (mean and SD are plotted) for the kinesthetic-visual w/ set-points (VI+S), kinesthetic-visual w/o set-points (VI), kinesthetic-vibratory w/ set-points (VB+S), and kinesthetic-vibratory w/o set-points (VI) conditions. Lower values of this metrics indicate higher performances in completing the given task.

means differed significantly among the feedback modalities ($F_{3,41.116} = 9.321, p < 0.001,\ a = 0.05$). Post-hoc analysis (Games-Howell post-hoc test) revealed statistically significant difference between groups VI+S and VB+S ($p = 0.025$), VB+S and VB ($p = 0.038$), VI+S and VI ($p = 0.046$), and VI and VB+S ($p < 0.001$). Moreover, although groups VI and VB were not found significantly different, comparison between them fell very short of significance ($p = 0.074$). No difference was revealed between VI+S and VB ($p = 0.999$).

Fig. 6b shows position error e_p for the four experimental conditions. The collected data passed Shapiro-Wilk normality test and Levene's homogeneity test. Comparison of the means among the feedback modalities was tested using one-way ANOVA. The means did not differed significantly among the feedback modalities ($F_{3,76} = 0.231, p = 0.875, a = 0.05$).

Fig. 6c shows orientation error e_o for the four experimental conditions. The collected data passed Shapiro-Wilk normality test and Levene's homogeneity test. Comparison of the means among the feedback modalities was tested using one-way ANOVA. The means differed significantly among the feedback modalities ($F_{3,76} = 8.047, p < 0.001, a = 0.05$). Post-hoc analysis (Tukey HSD post-hoc test) revealed statistically significant difference between groups VI+S and VB+S ($p = 0.043$) and VI and VB+S ($p < 0.001$). Moreover, although groups VI and VB were not found significantly different, comparison between them fell very short of significance ($p = 0.057$). No difference was revealed between the other groups (VI+S and VI, $p = 0.129$; VI+S and VB, $p = 0.984$; VB+S and VB, $p = 0.100$).

The experiment lasted 7.1 minutes on average. No difference between the conditions was observed in terms of task completion time.

5 Discussion and Future Works

Four experimental conditions were tested, considering two ways of computing ideal stimuli, i.e. with and without set-points (see Section 3.1), and two feedback modalities, i.e. kinesthetic-vibratory and kinesthetic-visual (see Section 3.2). The average error in reaching the target point e_t, and the average errors in following the ideal position and orientation signals, e_p and e_o, provided a measure of accuracy. Results are reported in Section 4.1 and Fig. 6. Targeting errors e_t and orientation errors e_o were lower for kinesthetic-vibratory conditions VB and VB+S with respect to kinesthetic-visual conditions VI and VI+S, respectively. Considering separately the two ways of computing ideal stimuli, vibratory feedback thus led to improved performance with respect to the visual one. On the other hand, as expected, no difference was found in position errors e_p. All the four experimental conditions, in fact, provided navigation cues about ideal position through kinesthetic force. It is also worth highlighting that, in general, following kinesthetic cues was much easier than following the vibratory ones, since the motors of the Omega actively pushed the end-effector toward the computed ideal position.

As expected, participants showed worse performance with respect to the autonomous controller presented by Abayazid et al. [6], where the steering algorithm controlled directly the slave robot achieving a mean targeting error e_t of 1.3 mm. However, the targeting accuracy achieved in our work is still sufficient to reach the smallest lesions detectable using state-of-art ultrasound imaging systems (ϕ 2 mm).

Work is in progress to evaluate the proposed teleoperation system in different clinically-relevant scenarios. We plan to test the proposed system with different target points, different algorithms to calculate ideal signals, introducing obstacles to avoid, and using biological tissue. Moreover, we will ask clinicians to be part of our next user study. We also plan to substitute kinesthetic feedback with stimuli of another sensory modality (e.g., cutaneous, audio), in order to make the system intrinsically passive [9] and safe, with no need of stability control. Finally, work is in progress to use kinesthetic force to provide clinicians with force feedback regarding the mechanical properties of the tissue being penetrated.

Acknowledgments

The research leading to these results has received funding from the Netherlands Organization for Scientific Research (NWO–Project: 11204) and from the European Union Seventh Framework Programme FP7/2007-2013 under grant agreement n° 270460 of the project "ACTIVE" and under grant agreement n° 601165 of the project "WEARHAP".

References

[1] N. Abolhassani, R. V. Patel, and M. Moallem, "Needle insertion into soft tissue: A survey," *Med. Eng. Phys.*, vol. 29, no. 4, pp. 413–431, 2007.
[2] C. Papalazarou, P. M. Rongen, and P. H. N. de With, "Surgical needle reconstruction using small-angle multi-view x-ray," in *Proc. IEEE Int. Conf. Image Process.*, 2010, pp. 4193–4196.
[3] V. Duindam, R. Alterovitz, S. Sastry, and K. Goldberg, "Screw-based motion planning for bevel-tip flexible needles in 3d environments with obstacles," in *Proc. IEEE Int. Conf. Robot. Autom.*, 2008, pp. 2483–2488.
[4] K. Hauser, R. Alterovitz, N. Chentanez, A. M. Okamura, and K. Goldberg, "Feedback control for steering needles through 3d deformable tissue using helical paths," presented at the Proc. Robot.: Sci. Syst., Seattle, WA, USA, 2009.
[5] M. Abayazid, R. J. Roesthuis, R. Reilink, and S. Misra, "Integrating deflection models and image feedback for real-time flexible needle steering," *IEEE Trans. Robot.*, vol. 29, no. 2, pp. 542–553, Apr. 2013.
[6] M. Abayazid, M. Kemp, and S. Misra, "3D flexible needle steering in soft-tissue phantoms using Fiber Bragg Grating sensors," in *Proc. IEEE Int. Conf. Robot. Autom.*, 2013, pp. 5823–5829.
[7] J. Troccaz and Y. Delnondedieu, "Semi-active guiding systems in surgery. a two-dof prototype of the passive arm with dynamic constraints (padyc)," *Mechatronics*, vol. 6, no. 4, pp. 399–421, 1996.
[8] M. Jakopec, F. Rodriguez y Baena, S. Harris, P. Gomes, J. Cobb, and B. L. Davies, "The hands-on orthopaedic robot "acrobot": Early clinical trials of total knee replacement surgery," *IEEE Trans. Robot. Autom.*, vol. 19, no. 5, pp. 902–911, Oct. 2003.
[9] D. Prattichizzo, C. Pacchierotti, and G. Rosati, "Cutaneous force feedback as a sensory subtraction technique in haptics," *IEEE Trans. Haptics*, vol. 5, no. 4, pp. 289–300, Fourth Quarter 2012.
[10] S. E. Salcudean, S. Ku, and G. Bell, "Performance measurement in scaled teleoperation for microsurgery," in *Proc. 1st Joint Conf. Comput. Vis., Virtual Reality Robot. Med. Med. Robot. Comput.-Assisted Surgery*, 1997, pp. 789–798.
[11] L. Meli, C. Pacchierotti, and D. Prattichizzo, "Sensory subtraction in robot-assisted surgery: fingertip skin deformation feedback to ensure safety and improve transparency in bimanual haptic interaction," *IEEE Trans. Biomed. Eng.*, vol. 61, no. 4, pp. 1318–1327, Apr. 2014.
[12] C. Pacchierotti, F. Chinello, M. Malvezzi, L. Meli, and D. Prattichizzo, "Two finger grasping simulation with cutaneous and kinesthetic force feedback," in *Proc. Int. Conf. Haptics: Perception, Devices, Mobility, Commun.*, 2012, pp. 373–382.
[13] C. Pacchierotti, A. Tirmizi, and D. Prattichizzo, "Improving transparency in teleoperation by means of cutaneous tactile force feedback," *ACM Trans. Appl. Perception*, vol. 11, no. 1, pp. 4:1–4:16, 2014.
[14] D. Prattichizzo, C. Pacchierotti, S. Cenci, K. Minamizawa, and G. Rosati, "Using a fingertip tactile device to substitute kinesthetic feedback in haptic interaction," in *Proc. Int. Conf. Haptics: Generating Perceiving Tangible Sensations*, 2010, pp. 125–130.
[15] C. R. Wagner, N. Stylopoulos, and R. D. Howe, "The role of force feedback in surgery: Analysis of blunt dissection," in *Proc. 10th Symp. Haptic Interfaces Virtual Envir. Teleoperator Syst.*, 2002, pp. 68–74.
[16] A. Kazi, "Operator performance in surgical telemanipulation," *Presence: Teleoperators Virtual Envir.*, vol. 10, no. 5, pp. 495–510, 2001.
[17] C. W. Kennedy, T. Hu, J. P. Desai, A. S. Wechsler, and J. Y. Kresh, "A novel approach to robotic cardiac surgery using haptics and vision," *Cardiovascular Eng.*, vol. 2, no. 1, pp. 15–22, 2002.
[18] M. Nakao, K. Imanishi, T. Kuroda, and H. Oyama, "Practical haptic navigation with clickable 3d region input interface for supporting master-slave type robotic surgery," *Stud. Health Technol. Informat.*, vol. 98, pp. 265–271, 2004.
[19] J. B. F. V. Erp, H. A. H. C. V. Veen, C. Jansen, and T. Dobbins, "Waypoint navigation with a vibrotactile waist belt," *ACM Trans. Appl. Perception*, vol. 2, no. 2, pp. 106–117, 2005.
[20] K. Kuchenbecker, J. Gewirtz, W. McMahan, D. Standish, P. Martin, J. Bohren, P. Mendoza, and D. Lee, "Verrotouch: High-frequency acceleration feedback for telerobotic surgery," in *Proc. Haptics: Generating Perceiving Tangible Sensations*, 2010, pp. 189–196.

[21] G. J. Vrooijink, M. Abayazid, and S. Misra, "Real-time three-dimensional flexible needle tracking using two-dimensional ultrasound," in *Proc. IEEE Int. Conf. Robot. Autom.*, 2013, pp. 1680–1685.
[22] M. Franken, S. Stramigioli, S. Misra, C. Secchi, and A. Macchelli, "Bilateral telemanipulation with time delays: A two-layer approach combining passivity and transparency," *IEEE Trans. Robot.*, vol. 27, no. 4, pp. 741–756, Aug. 2011.
[23] M. Abayazid, G. J. Vrooijink, S. Patil, R. Alterovitz, and S. Misra, "Experimental evaluation of ultrasound-guided 3d needle steering in biological tissue," *Int. J. Comput. Assisted Radiol. Surgery*, pp. 1–9, Feb. 2014.
[24] R. W. Cholewiak and A. A. Collins, "Sensory and physiological bases of touch," in *The Psychology of Touch*, M. A. Heller, and W. Schiff, Eds. Hillside, England: Laurence Erlbaum Assoc., 1991, pp. 13–60.
[25] K. A. Kaczmarek, J. G. Webster, P. Bach-y Rita, and W. J. Tompkins, "Electrotactile and vibrotactile displays for sensory substitution systems," *IEEE Trans. Biomed. Eng.*, vol. 38, no. 1, pp. 1–16, Jan. 1991.
[26] H. Pongrac, "Vibrotactile perception: Examining the coding of vibrations and the just noticeable difference under various conditions," *Multimedia Syst.*, vol. 13, no. 4, pp. 297–307, 2008.